IOP Publishing Journal of Physics D: Applied Physics

J. Phys. D: Appl. Phys. **49** (2016) 045306 (7pp) doi:10.1088/0022-3727/49/4/045306

Transport gap in vertical devices made of incommensurately misoriented graphene layers

V Hung Nguyen[1,2] and P Dollfus[1]

[1] Institut d'Electronique Fondamentale, CNRS, Univ. Paris-Sud, Université Paris-Saclay, 91405 Orsay, France
[2] Center for Computational Physics, Institute of Physics, Vietnam Academy of Science and Technology, PO Box 429 Bo Ho, 10000 Hanoi, Vietnam

E-mail: hung@iop.vast.ac.vn

Received 20 July 2015, revised 24 November 2015
Accepted for publication 26 November 2015
Published 22 December 2015

Abstract

By means of atomistic tight-binding calculations, we investigate the transport properties of vertical devices made of two incommensurately misoriented graphene layers. For a given transport direction (*Ox*-axis), we define two classes of rotated graphene lattice distinguished by difference in lattice symmetry and, hence, in Brillouin zone. In particular, these two classes correspond to two different cases where the position of their Dirac cones in the k_y-axis is determined differently, i.e. $K'_y = K_y = 0$ or $K'_y = -K_y = 2\pi/3L_y$ (L_y is the periodic length along the *Oy* axis). As a consequence, in devices made of two layers of different lattice classes, the misalignment of Dirac cones between the left and right graphene sections opens a finite energy-gap of conductance that can reach a few hundreds of meV. We also show that strain engineering can be used to further enlarge the transport gap and to diminish the sensitivity of the gap on the twist angle and on the commensurateness of the layer stack.

Keywords: energy gap, graphene, tight binding approach

(Some figures may appear in colour only in the online journal)

Graphene is nowadays one of the most attractive materials in several research fields because of its unusual, and in many respects, excellent physical properties, as a consequence of its two-dimensional honeycomb lattice. In particular, it is expected to be a good channel material in high-frequency electronic devices, flexible devices, spintronic devices, and to provide outstanding properties for photonics and optoelectronics, sensors, energy storage and conversion and so on [1]. However, with a view to digital applications in electronics, the lack of bandgap in graphene is known to make it difficult to turn off the current of transistors leading to low I_{ON}/I_{OFF} ratio and poor current saturation [2, 3], which is a strong limitation for practical applications. So far, many efforts in engineering bandgap in graphene have been made to solve this issue. For instance, techniques such as cutting 2D graphene sheets into narrow nanoribbons [4], depositing graphene on hexagonal boron nitride substrate [5], nitrogen-doped graphene [6], applying an electric field perpendicularly to Bernal-stacking bilayer graphene [7], graphene nanomeshes [8], using hybrid graphene/hexagonal boron-nitride [9] or vertical graphene channels [10] have been explored. Although they are certainly promising options for opening a bandgap in graphene, some of them have their own drawbacks while the others still need experimental verification and realization. Hence, bandgap engineering is still a timely topic for the development of graphene in nanoelectronics.

In this context, it has been also shown that the lattice orientation is an additional degree of freedom to control the electronic properties of graphene channels. In particular, one can rotate one graphene layer with respect to the other ones in few-layer graphene systems (i.e. twisted few-layer graphene lattices) to form graphene-on-graphene moiré patterns, which allows us to strongly modulate their electronic structure. Indeed, the bandstructure of twisted graphene bilayers changes dramatically [11–14], compared to that of Bernal/AA stacking bilayer systems. In addition to the linear

 © 2016 IOP Publishing Ltd Printed in the UK

dispersion in the vicinity of *K*-points, saddle points emerge at the crossing of Dirac cones (i.e. at the *M*-point in the Brillouin zone), yielding van Hove singularities in the density of states at low energies and remarkable renormalization of the Fermi velocity. Moreover, several properties (e.g. magnetic, optical, phonon transport etc...) are strongly modified when tuning the twist angle [14–17]. The dependence of conductance on the twist angle in misoriented graphene multilayers has been also investigated in a number of works, e.g. in [18–21]. Especially, controlling the orientation of graphene layers has been demonstrated as a good strategy to modulate the resonant tunneling effects and non-linear transport characteristics in graphene/hexagonal boron-nitride/graphene heterostructures [22–24].

It is worth mentioning that recently, many researches in graphene-based electronics are being oriented toward devices made of vertical heterostructures of graphene and other layered materials [10, 22–32]. This new direction lies on the fact that inserting large bandgap layers between graphene sheets is an effective strategy to solve the main drawback of graphene, i.e. its gapless character, which makes it possible to block the current in the OFF state of graphene devices. Indeed, the ON/OFF current ratio in vertical graphene devices is significantly improved, compared to that in the case of pristine graphene channel [10, 26–30]. However, these vertical heterochannels still need further optimization so as to solve the issues related to the combination of the different materials and to further improve other figures of merit as switching frequency and delay time [29].

In this regard, we have recently investigated and proposed to use the vertical channels based on two misoriented graphene layers only [33]. The idea was to exploit the possibility of opening a finite energy gap of transmission through the channel thanks to the mismatch between the band-structures of the two graphene layers. We have demonstrated that a large energy gap of a few hundreds meV can be obtained when the channel is strained. It is essentially a consequence of the orientation-dependence of electronic structure of graphene layers that leads to the non-coincidence of their Dirac cones in the *k*-space and hence a finite transport gap when a strain is applied. Similarly, the origin of this energy-gap has been also explained in detail in [34, 35]. It is very different in nature from the bandgap in other graphene nanostructures (e.g. the bandgap induced by a perpendicular electric field in graphene bilayers [7]) since both graphene layers are still semi-metallic. With a large energy-gap induced by a small strain of only a few percents, this type of graphene heterochannels is very promising for applications as strain sensors and flexible graphene transistors. Experimentally, controlling the misorientation of graphene layers has been also demonstrated as an efficient strategy to modulate the electronic properties of the vertical heterochannels, e.g. in graphene/hexagonal boron-nitride/graphene heterostructures [24], graphene on top of hexagonal boron-nitride [36], etc... The heterochannels in [33] may have an advantage in terms of fabrication process, compared to the vertical heterochannels mentioned above, since they are formed of graphene layers only. However, in this previous study, only devices made of commensurate layers were investigated. Actually, the commensurate systems occur only for a set of well controlled twist angles, which can still be an issue for the fabrication in practice, while the incommensurate ones are more common. It naturally gives rise to a question about the transport properties of channels made of incommensurate layers and answering this question is our aim in the current work. Additionally, even if the two layers in the commensurate systems have different orientations, their Dirac cones are still at the same position in the *k*-space, which leads to a zero energy gap, if strain is not applied. We will demonstrate here that this issue can be solved in the case of incommensurate layers and, on this basis, we will explore the new possibilities of energy-gap engineering in this type of vertical graphene hetero-channels.

The studied structures are schematized in figure 1. They consist in two partially overlaped graphene layers and we assume additionally that the overlap region has two edges perpendicular to the transport (*Ox*) direction. The top layer is rotated relatively to the bottom one by an angle ϕ_{TL} but, differently from the study in [33], they are incommensurate layers, i.e. they do not have any common (truly) periodic lattice vector. Here, we consider 2D graphene channels, i.e. the width of graphene layers is very large, or, in other words, assumed to be infinite. Hence, to carry out the calculations, the periodicity of the channel along the transverse (*Oy*) direction is a necessary assumption [33–35]. In this regard, we propose to make an approximation as follows. In all incommensurate cases, the two layers have different lengths L_y^1 and L_y^2 of unit cells along the *Oy* axis. However, when they are coupled to form a heterochannel, we can always find two periodic vectors $\tilde{\mathbf{L}}_y^1 = m_1\mathbf{L}_y^1$ and $\tilde{\mathbf{L}}_y^2 = m_2\mathbf{L}_y^2$ that satisfy the condition $\tilde{L}_y^1 \simeq \tilde{L}_y^2$. Our calculations are thus performed similarly as in [33–35] with an approximate periodic length $\tilde{L}_y = (\tilde{L}_y^1 + \tilde{L}_y^2)/2$. This approximation can be reasonably accepted if the difference between $\tilde{L}_y^1$ and $\tilde{L}_y^2$ is small enough, as it has been confirmed in similar systems [27, 37–41]. In particular, in studies on graphene grain boundaries [37–39], it was shown that tight binding calculations made within the above approximation are in good agreement with density functional theory, especially in the region close to the energy-gap. The transport properties have been accurately computed around the gap even when the difference between $\tilde{L}_y^1$ and $\tilde{L}_y^2$ reaches ~3.85%. Similar agreement has been obtained in graphene/hBN heterochannels [27, 40, 41], where the lattice mismatch is about 1.8%. Throughout the present work, to ensure good accuracy, our calculations for all structures were hence performed with $\tilde{L}_y^1$ and $\tilde{L}_y^2$ that have only a small difference, i.e. <2%.

Now, we would like to explain the nomenclature of graphene lattices considered in this work. In figure 1, we plot the geometry of two typical devices, i.e. the left (bottom) layer has zigzag and armchair orientation in (a) and (b), respectively, with respect to the *Ox* axis. We distinguish two lattice types as follows. For both cases, the lattice is determined by rotating the original (zigzag or armchair) lattice by an angle ϕ_{TL}. This angle is computed as $\cos\phi_{\mathrm{TL}} = \frac{\mathbf{L_y}\cdot\mathbf{L_y^0}}{\|\mathbf{L_y}\|\|\mathbf{L_y^0}\|}$ where $\mathbf{L_y}$ is the vector (before the lattice is rotated) defining

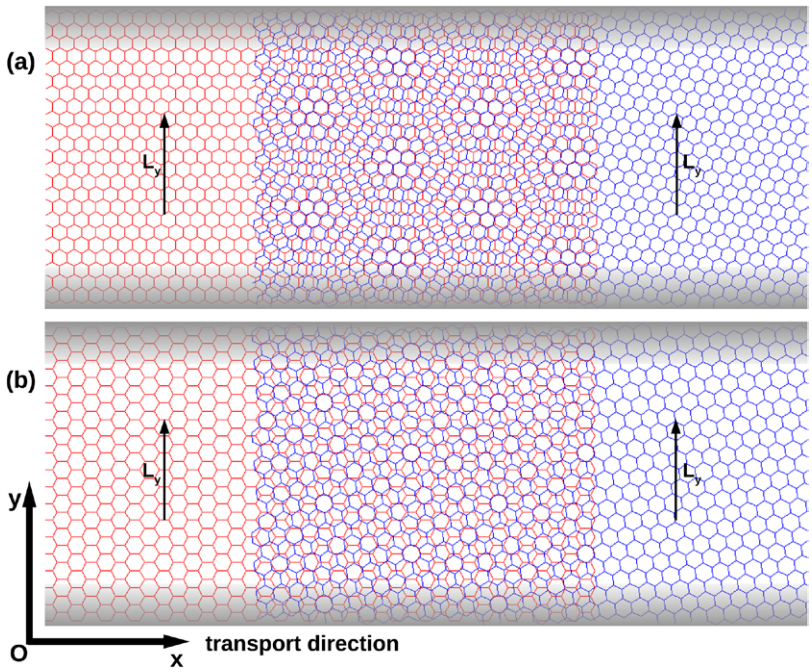

Figure 1. Schematic of devices made of vertical stack of misoriented graphene layers. The left layer has a zigzag (a) or amrchair orientation (b) along the transport direction.

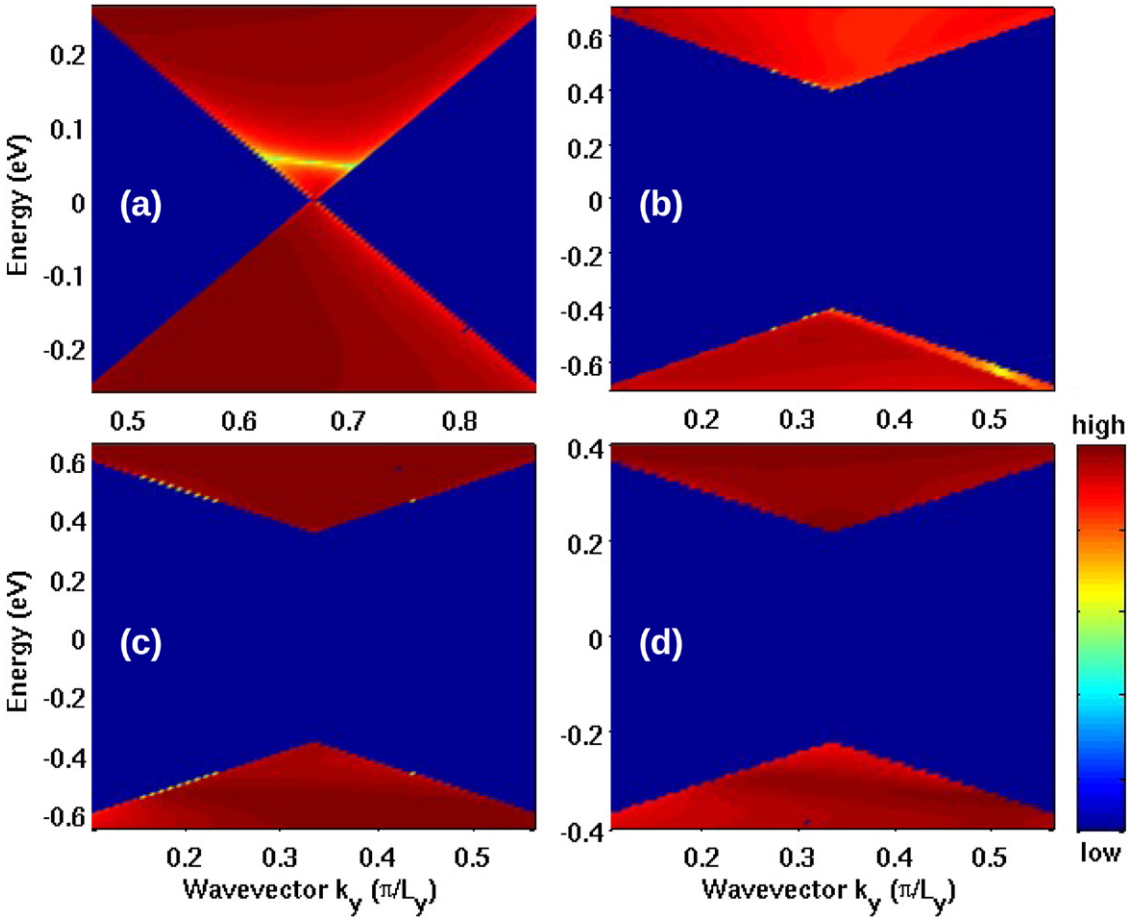

Figure 2. $(E - k_y)$-maps of transmission probability around the neutrality (Dirac) point in different devices. The devices made of $(AM_{7,4}@AM_{4,7})$, $(AM_{6,6}@AM_{7,4})$, $(ZZ_{4,4}@ZZ_{5,3})$, $(AM_{13,7}@AM_{13,8})$ layers are considered in the panels (a),(b),(c) and (d), respectively (see the definition of layers in the text).

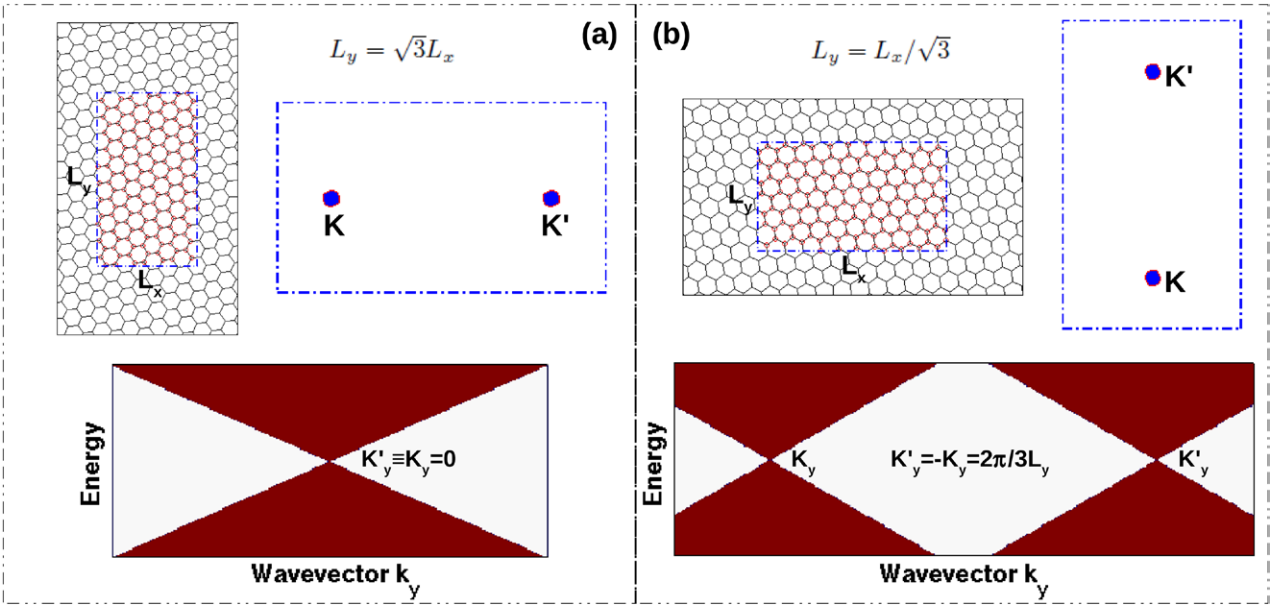

Figure 3. Schematic of two typical periodic cells of graphene lattices, shape of their Brillouin zone, and corresponding pictures showing their bandstructure profile along the k_y axis.

the size of unit cells along the Oy-axis while $\mathbf{L_y^0}$ is the vector of the original lattice. These vectors are determined as $\mathbf{L_y} = q_1\mathbf{a_1} + q_2\mathbf{a_2}$ and $\mathbf{L_y^0} = \mathbf{a_1} + \mathbf{a_2}$. For the type 1 (i.e. $ZZ_{q1,\,q2}$ lattice, see in figure 1(a)) when the original lattice has a zigzag orientation along the Ox axis, $\mathbf{a_1} = \left(-\sqrt{3}, 3\right)a_0/2$ and $\mathbf{a_2} = \left(\sqrt{3}, 3\right)a_0/2$. For the type 2 (i.e. $AM_{q1,\,q2}$ lattice, see in figure 1(b)) when the original lattice has an armchair orientation, $\mathbf{a_1} = \left(-3, \sqrt{3}\right)a_0/2$ and $\mathbf{a_2} = \left(3, \sqrt{3}\right)a_0/2$. Here, $a_0 = 0.142\,\text{nm}$ is the in-plane C-C bond length in graphene. Accordingly, we determine also the size of unit cells along the Ox axis as $\mathbf{L_x} = p_1\mathbf{a_1} + p_2\mathbf{a_2}$ that satisfies the condition $\mathbf{L}_x \cdot \mathbf{L}_y = 0$, i.e. $\frac{p_1}{p_2} = -\frac{2q_2+q_1}{2q_1+q_2}$ and $\frac{p_1}{p_2} = -\frac{2q_2-q_1}{2q_1-q_2}$ for $ZZ_{q1,\,q2}$ and $AM_{q1,\,q2}$ lattices, respectively.

To compute the electronic transport in the considered systems, we employed atomistic tight-binding calculations and Green's function techniques as in [33–35, 42–45]. In particular, the hopping parameters are determined similarly as in [42–45], i.e. $t_{ij} = t_0 \exp\left[-\beta\{r_{ij}/r_0 - 1\}\right]$ where $t_0 = -2.7\,\text{eV}$ (resp. 0.48 eV), $\beta = 3.37$ (resp. 7.42) and $r_0 = 1.42$ Å $\equiv a_0$ (resp. 3.35 Å) for in-plane (resp. interlayer) interactions.

First, we would like to analyze some basic transport properties of the considered devices. We display in figure 2 the $(E - k_y)$-maps of transmision probability in four cases: the devices made of ($AM_{7,4}$@$AM_{4,7}$), ($AM_{6,6}$@$AM_{7,4}$), ($ZZ_{4,4}$@$ZZ_{5,3}$), ($AM_{13,7}$@$AM_{13,8}$) layers in the panels (a)–(d), respectively. Note that the two layers $AM_{7,\,4}$ and $AM_{4,\,7}$ are commensurate while the other systems are incommensurate. It is clearly shown that in the case of commensurate lattices, even if the two lattices have different orientations, there is no energy-gap of transmission. This can be explained by the fact that the commensurate lattices have the same periodic vectors and hence, because of their same lattice symmetry, they have the same Brillouin zone. Since their Dirac cones are located at the same k-point, the transport gap is zero, similarly as reported in [33, 38, 45]. The transport picture, however, can be dramatically changed in the devices made of incommensurate layers, i.e. finite energy-gaps can be achieved as shown in figures 2(b)–(d). The value of energy-gap is quite significant in these cases: $E_g \simeq 810.6$ meV in (b), 703.2 meV in (c), and 432.8 meV in (d). This phenomenon is explained as follows. For all cases studied, we can distinguish two classes of rotated graphene lattice as shown in figures 3(a) and (b). In the class 1, the lengths L_x and L_y determining the unit (smallest

Table 1. Description of some concrete devices investigated in this work and their transport gap E_g.

Layer 1	Layer 2	ϕ_{TL}	$\tilde{L}_y$ (a_0)	η (%)	E_g (meV)
$ZZ_{4,\,4}$	$ZZ_{5,\,3}$	8.21°	12.062	1.031	703.2
$ZZ_{5,\,5}$	$ZZ_{8,\,1}$	24.18°	14.899	1.351	569.3
$ZZ_{13,\,1}$	$ZZ_{11,\,4}$	11.25°	23.366	0.549	363.0
$ZZ_{8,\,8}$	$ZZ_{13,\,2}$	22.94°	24.216	1.790	350.2
$ZZ_{15,\,1}$	$ZZ_{13,\,4}$	9.80°	26.776	0.836	316.7
$ZZ_{19,\,1}$	$ZZ_{17,\,4}$	7.78°	33.629	1.061	252.2
$AM_{6,\,6}$	$AM_{7,\,4}$	25.28°	10.464	1.369	810.6
$AM_{9,\,9}$	$AM_{10,\,7}$	16.99°	15.491	1.250	547.5
$AM_{13,\,7}$	$AM_{13,\,8}$	5.04°	19.595	0.781	432.8
$AM_{14,\,9}$	$AM_{13,\,11}$	12.41°	21.141	1.342	401.2
$AM_{14,\,14}$	$AM_{16,\,11}$	17.78°	24.402	1.259	347.6
$AM_{17,\,9}$	$AM_{17,\,10}$	3.87°	25.573	0.458	331.6
$ZZ_{11,\,4}$	$AM_{14,\,13}$	18.59°	23.366	0.549	362.9
$ZZ_{13,\,2}$	$AM_{16,\,11}$	24.83°	24.494	0.500	346.2
$ZZ_{15,\,1}$	$AM_{17,\,13}$	16.20°	26.776	0.836	316.7
$ZZ_{15,\,4}$	$AM_{19,\,14}$	26.22°	29.798	1.689	284.6

Note: Here, ϕ_{TL} is the twist angle, $\tilde{L}_y$ is the average periodic length along the Oy axis, and η indicates the mismatch between $\tilde{L}_y^1$ and $\tilde{L}_y^2$ of the two layers.

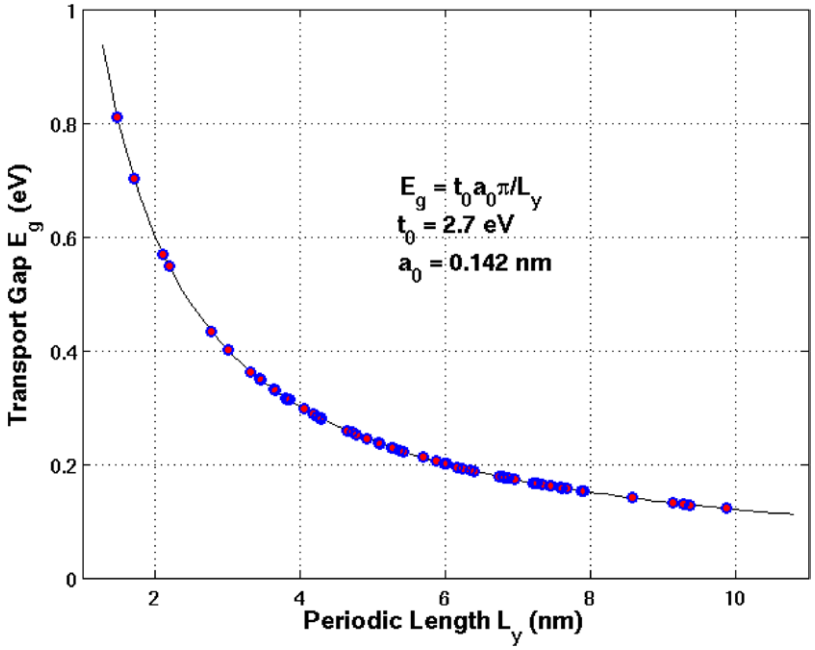

Figure 4. Transport gap as a function of periodic length $\tilde{L}_y$ along the Oy axis.

periodic) cell satisfy $L_y = \sqrt{3}L_x$ while $L_y = L_x/\sqrt{3}$ for the class 2. Accordingly, the Brillouin zone and Dirac cones (at the K-points) of these two lattice classes have different properties: $K'_y = K_y = 0$ for the class 1 while $K'_y = -K_y = 2\pi/3L_y$ for the class 2, as schematized in figure 3. Similarly to the case of commensurate lattices, if the channel is made of two layers of the same class, the Dirac cones of both layers are located at the same k-points and the transport gap is zero (not shown). However, if the channel is made of layers of different classes, the misalignment of their Dirac cones in the k-space generates a finite transport gap, which explains the results obtained.

In the table 1, we show the detailed description of some concrete devices investigated in this work and their transport gap. $\tilde{L}_y$ is the average periodic length of two layers along the Oy axis and η denotes the mismatch between $\tilde{L}^1_y$ and $\tilde{L}^2_y$, i.e. $\eta = |\tilde{L}^1_y - \tilde{L}^2_y|/\tilde{L}_y$. As mentioned above, our calculations were performed with $\eta < 2\%$ in all cases. First, we find that there are various possibilities of finite energy-gap using this design strategy and E_g can reach a few hundreds meV. Important, the dependence of E_g on the twist angle is quite complicated but E_g is simply inversely proportional to $\tilde{L}_y$. This is essentially explained as follows. The value of E_g is basically proportional to the distance ΔK_y between the Dirac cones of the two layers along the k_y-axis [33, 35, 38]. In the considered channels, ΔK_y is actually equal to $2\pi/3\tilde{L}_y$, which fully explains the property above. On this basis, we can also analytically compute the value of E_g. Note that in the low energy regime (i.e. $|E| \ll 1$ eV around the Dirac point), the energy dispersion of graphene is well described by the simple formula $E(\tilde{k}) = \pm \hbar v_F \tilde{k}$ with $v_F = 3a_0t_0/2\hbar$ and $\tilde{\mathbf{k}} = \mathbf{k} - \mathbf{K}$ (i.e. $t_0 = 2.7$ eV and $a_0 = 0.142$ nm). The bandegde is thus defined as a function of $\tilde{k}_y$ as $E_{edge}(\tilde{k}_y) = \pm 3t_0a_0|\tilde{k}_y|/2$. In the considered channel, the Dirac cones of the two layers are located at different k_y-points, i.e. at $K^1_y = 0$ and $K^2_y = 2\pi/3\tilde{L}_y$, respectively, and the energy-gap is thus determined as the value of $E_{edge}(\tilde{k}_y)$ at the middle point [33, 35, 38], i.e. $\tilde{k}_y = \pi/3\tilde{L}_y$ (see also in figures 2(b)–(d)). Hence, we have

$$E_g \simeq \pi \frac{a_0}{\tilde{L}_y} t_0 \tag{1}$$

In figure 4, we summarize the results obtained in all studied devices. They indeed confirm an excellent agreement with the analytical formula above.

Now, new questions arise. Since the dependence of E_g on the twist angle is quite complicated, it shall not be easy to control well this energy-gap in practice. Additionally, the control of the commensurateness of the two layers is also an open question. To partly solve these issues, we propose to use strain engineering as an additional ingredient. As suggested in [33], the strain effects are very efficient to open a finite transport-gap in devices made of commensurate lattices. Similarly, this idea can be used here to open an energy-gap in the channels where two incommensurate layers are of the same lattice class, i.e. when $E_g = 0$ without strain. Additionally, in the cases of device with a small gap (i.e. if the two layers are from different lattice classes and $\tilde{L}_y$ is large), strain can be used to further enlarge E_g. These points are clearly shown in figure 5 for three typical cases: commensurate ($AM_{7,\ 4}$@$AM_{4,\ 7}$), incommensurate ($AM_{14,\ 14}$@$AM_{9,\ 16}$) with zero gap and incommensurate ($AM_{11,\ 20}$@$AM_{13,\ 20}$) with a small gap if no strain is applied. The gap is significantly broadened, i.e. by a few hundreds meV, when a small strain of only 4% is applied.

In conclusion, we have investigated the transport properties of vertical devices made of two incommensurately misoriented graphene layers. For given Oxy coordinates with

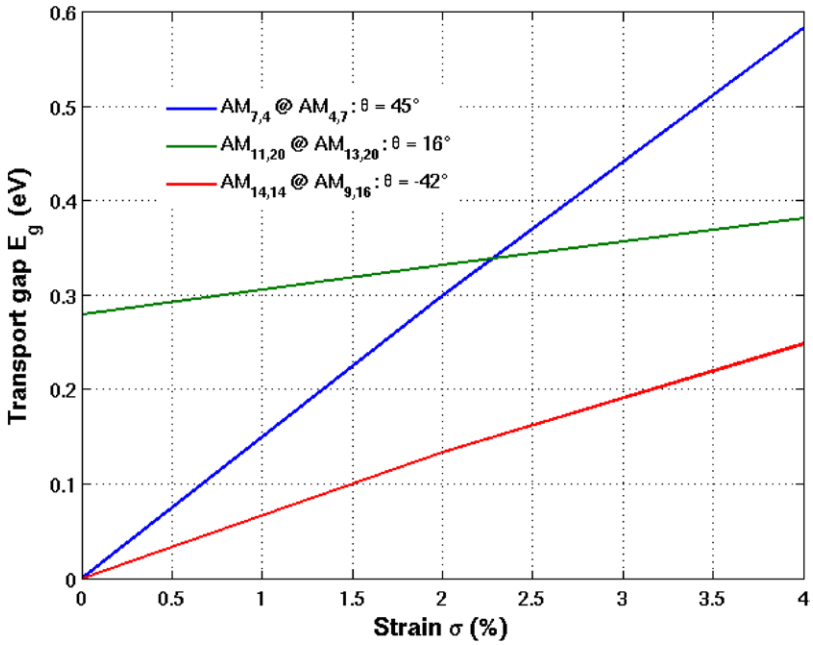

Figure 5. Strain effects on the transport gap in different devices. The strain of angle θ with respect to the transport direction (Ox) is applied [33].

transport direction parallel to the Ox axis, there are two different classes of graphene lattice depending on their lattice symmetry and on the properties of their Brillouin zone. In particular, depending on the graphene lattices, the two Dirac cones are either located at the same k_y-point ($K'_y = K_y = 0$) or at different k_y-points ($K'_y = -K_y = 2\pi/3L_y$). As a consequence, in devices made of two layers of different lattice classes, the misalignment of Dirac cones of the two layers leads to a significant energy-gap (i.e. a few hundreds of meV) of conductance. The gap is shown to be inversely proportional to the length L_y. We have also shown the possibility of using strain to enlarge the energy-gap and to diminish the sensitivity of the gap on the twist angle and commensurateness of the layer stack. Thus, our study suggests an alternative strategy to open an energy gap in graphene channels without altering the graphene lattices, by controlling the misorientation of two partially overlapped graphene layers, which should be helpful for broadening the practical applications of graphene.

Acknowledgments

This research in Hanoi is funded by Vietnam's National Foundation for Science and Technology Development (NAFOSTED) under grant number 103.01-2014.24.

References

[1] Ferrari A C *et al* 2015 *Nanoscale* **7** 4598–810
[2] Meric I, Han M Y, Young A F, Ozyilmaz B, Kim P and Shepard K L 2008 *Nat. Nanotechnol.* **3** 654–9
[3] Alarcón A, Hung Nguyen V, Berrada S, Querlioz D, Saint-Martin J, Bournel A and Dollfus P 2013 *IEEE Trans. Electron Devices* **60** 985–91
[4] Han M Y, Özyilmaz B, Zhang Y and Kim P 2007 *Phys. Rev. Lett.* **98** 206805
[5] Kharche N and Nayak S K 2011 *Nano Lett.* **11** 5274–78
Tang S *et al* 2013 *Sci. Rep.* **3** 2666
[6] Lherbier A *et al* 2013 *Nano Lett.* **13** 1446–50
Zabet-Khosousi A *et al* 2014 *J. Am. Chem. Soc.* **136** 1391–7
[7] Zhang Y, Tang T-T, Girit C, Hao Z, Martin M C, Zettl A, Crommie M F, Shen Y R and Wang F 2009 *Nature* **459** 820–3
[8] Bai J, Zhong X, Jiang S, Huang Y and Duan X 2010 *Nat. Nanotechnol.* **5** 190–4
[9] Fiori G, Betti A, Bruzzone S and Iannaccone G 2012 *ACS Nano* **6** 2642–8
[10] Britnell L *et al* 2012 *Science* **335** 947–50
Yu W J *et al* 2013 *Nat. Nanotechnol.* **8** 952–8
[11] Lopes dos Santos J M B, Peres N M R and Castro A H 2007 *Phys. Rev. Lett.* **99** 256802
[12] Brihuega I *et al* 2012 *Phys. Rev. Lett.* **109** 196802
[13] Yan W *et al* 2013 *Nat. Commun.* **4** 2159
[14] Moon P and Koshino M 2012 *Phys. Rev.* B **85** 195458
[15] Stauber T, San-Jose P and Brey L 2013 *New J. Phys.* **15** 113050
[16] Moon P and Koshino M 2013 *Phys. Rev.* B **88** 241412
[17] Cocemasov A I *et al* 2013 *Phys. Rev.* B **88** 035428
Nika D L *et al* 2014 *Appl. Phys. Lett.* **105** 031904
[18] Bistritzer R and MacDonald A H 2010 *Phys. Rev.* B **81** 245412
[19] Masum K M, Sylvia S S, Ge S, Neupane M and Lake R K 2013 *Appl. Phys. Lett.* **103** 243114
[20] He W-Y, Chu Z-D and He L 2013 *Phys. Rev. Lett.* **111** 066803
[21] Qiao J-B and He L 2014 *Phys. Rev.* B **90** 075410
[22] Brey L 2014 *Phys. Rev. Appl.* **2** 014003
[23] Britnell L *et al* 2013 *Nat. Commun.* **4** 1794
[24] Mishchenko A *et al* 2014 *Nat. Nanotechnol.* **9** 808–13
[25] Bala Kumar S, Seol G and Guo J 2012 *Appl. Phys. Lett.* **101** 033503
[26] Georgiou T *et al* 2013 *Nat. Nanotechnol.* **8** 100–3
[27] Fiori G, Bruzzone S and Iannaccone G 2013 *IEEE Trans. Electron Devices* **60** 268–73
[28] Moriya R *et al* 2014 *Appl. Phys. Lett.* **105** 083119
[29] Logoteta D, Fiori G and Iannaccone G 2014 *Sci. Rep.* **4** 6607

[30] Das T, Jang H, Lee J B, Chu H, Kim S D and Ahn J-H 2015 *2D Mater* **2** 044006
[31] Zhang Q, Fiori G and Iannaccone G 2014 *IEEE Electron Device Lett.* **35** 966–8
[32] Bruzzone S, Logoteta D, Fiori G and Iannaccone G 2015 *Sci. Rep.* **5** 14519
[33] Hung Nguyen V, Viet Nguyen H, Saint-Martin J and Dollfus P 2015 *Nanotechnology* **26** 115201
[34] Hung Nguyen V, Viet Nguyen H, Saint-Martin J and Dollfus P 2014 *Nanotechnology* **26** 165201
[35] Chung Nguyen M, Hung Nguyen V, Viet Nguyen H and Dollfus P 2014 *Semicond. Sci. Technol.* **29** 115024
[36] Woods C R *et al* 2014 *Nat. Phys.* **10** 451–6
[37] Yazyev O V and Louie S G 2010 *Nat. Mater.* **9** 806–9
[38] Kumar S B and Guo J 2012 *Nano Lett.* **12** 1362–6
[39] Zhang J, Gao J, Liu L and Zhao J 2012 *J. Appl. Phys.* **112** 053713
[40] Moon P and Koshino M 2014 *Phys. Rev.* B **90** 155406
[41] Seol G and Guo J 2011 *Appl. Phys. Lett.* **98** 143107
[42] Pereira V M, Castro A H and Peres N M R 2009 *Phys. Rev.* B **80** 045401
[43] Wang Z F, Liu F and Chou M Y 2012 *Nano Lett.* **12** 3833–8
[44] Koshino M 2015 *New J. Phys.* **17** 015014
[45] Hung Nguyen V and P Dollfus 2015 *2D Mater* **2** 035005